Optical and Electron Spin Resonance Studies of Xenon–Nitrogen–Helium Condensates Containing Nitrogen and Oxygen Atoms

ARTICLE *in* THE JOURNAL OF PHYSICAL CHEMISTRY A · MARCH 2015

Impact Factor: 2.69 · DOI: 10.1021/jp508534t · Source: PubMed

10 AUTHORS, INCLUDING:

Roman Boltnev
Russian Academy of Sciences
38 PUBLICATIONS **366** CITATIONS
SEE PROFILE

Vladimir V Khmelenko
Texas A&M University
98 PUBLICATIONS **792** CITATIONS
SEE PROFILE

Adil Meraki
Texas A&M University
5 PUBLICATIONS **8** CITATIONS
SEE PROFILE

THE JOURNAL OF PHYSICAL CHEMISTRY A

Article

pubs.acs.org/JPCA

Optical and Electron Spin Resonance Studies of Xenon–Nitrogen–Helium Condensates Containing Nitrogen and Oxygen Atoms

Roman E. Boltnev,[†,‡] Igor B. Bykhalo,[†] Irina N. Krushinskaya,[†] Alexander A. Pelmenev,[†,‡] Vladimir V. Khmelenko,*[,§] Shun Mao,[§] Adil Meraki,[§] Scott C. Wilde,[§] Patrick T. McColgan,[§] and David M. Lee[§]

[†]Branch of Talroze Institute for Energy Problems of Chemical Physics, Russian Academy of Sciences, Chernogolovka 142432, Russia

[‡]Joint Institute for High Temperatures, Russian Academy of Sciences, Moscow 125412, Russia

[§]Institute for Quantum Science and Engineering, Department of Physics and Astronomy, Texas A&M University, College Station, Texas 77843, United States

ABSTRACT: We present the first observations of excimer XeO* molecules in molecular nitrogen films surrounding xenon cores of nanoclusters. Multishell nanoclusters form upon the fast cooling of a helium jet containing small admixtures of nitrogen and xenon by cold helium vapor (T = 1.5 K). Such nanoclusters injected into superfluid helium aggregate into porous impurity–helium condensates. Passage of helium gas with admixtures through a radio frequency discharge allows the storage of high densities of radicals stabilized in impurity–helium condensates. Intense recombination of the radicals occurs during destruction of such condensates and generates excited species observable because of optical emission. Rich spectra of xenon–oxygen complexes have been detected upon destruction of xenon–nitrogen–helium condensates. A xenon environment quenches metastable N(^{2}D) atoms but has a much weaker effect on the luminescence of N(^{2}P) atoms. Electron spin resonance spectra of N(^{4}S) atoms trapped in xenon–nitrogen–helium condensates have been studied. High local concentrations of nitrogen atoms (up to 10^{21} cm^{-3}) stabilized in xenon–nitrogen nanoclusters have been revealed.

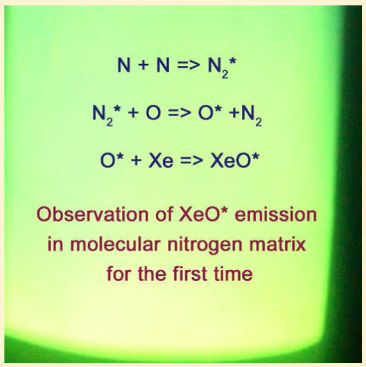

1. INTRODUCTION

Emissions from excimer XeO* molecules have been observed and extensively studied in both gaseous[1−4] and condensed[5−11] phases. Up to now, experiments with XeO* in condensed phases were limited to solid and liquid rare gas (RG) matrices. Beams of electrons, α-particles, or protons, as well as ultraviolet (UV) irradiation (with wavelengths of 260 nm and shorter) were used to form excited xenon–oxygen complexes in neon, argon, or krypton matrices doped with xenon atoms and O_2, N_2O, or CO_2 molecules as precursors of oxygen atoms. It is worth noting that excitation of a xenon matrix doped with O atoms causes an emission with a much simpler spectrum. It consists of two intense bands with maxima at 370 and 740 nm,[8,12] on the edges of the visible range.

In earlier work, the "green bands" of XeO* molecule were detected upon destruction of impurity–helium condensates consisting of impurity nanoclusters formed by nitrogen, neon, and xenon atoms and N_2 molecules.[13] The spectrum detected was similar to others observed from RG matrices, but two questions from previous investigations remained unanswered: where did the emitting XeO* molecules reside and what processes were responsible for their excitation? Impurity–helium condensates (IHCs) are formed in bulk superfluid helium (HeII) by aggregation of impurity nanoclusters injected by a gaseous helium jet.[14] The nanoclusters grow upon cooling of the helium jet containing ∼1% impurity (for instance, atoms of Ne, Ar, Kr, Xe, molecules of hydrogen, deuterium, nitrogen). H, D, and N atoms are obtained in an impurity–helium jet after passage through a radio frequency (RF) discharge region. The sizes of the nanoclusters are of order 5–6 nm, and they contain typically 2500–5000 atoms and molecules.[14] Multishell nanoclusters form in a helium jet for the case of admixtures of impurities with different binding energies.[15−18] As an example, during condensation of a nitrogen–neon–xenon–helium gas jet, the multishell nanoclusters are formed in which Xe cores are covered by three successive shells composed of different impurities in the following order: N_2 shell, Ne shell, and finally solid He shell. Each shell contains a small amount of other species presented in the jet.[15,17] Formation of clusters with similar multishell structures was also observed in supersonic jets.[19,20] In this work we report new results obtained in spectroscopic studies of luminescence observed during destruction of xenon–nitrogen–helium condensates. Decreasing the xenon content in the condensates was accompanied by transformations of the luminescence spectra detected: rich spectra of xenon–oxygen complexes had been detected upon destruction of the condensates with a low content of xenon,

Special Issue: Markku Räsänen Festschrift

Received: August 23, 2014
Revised: October 27, 2014
Published: October 29, 2014

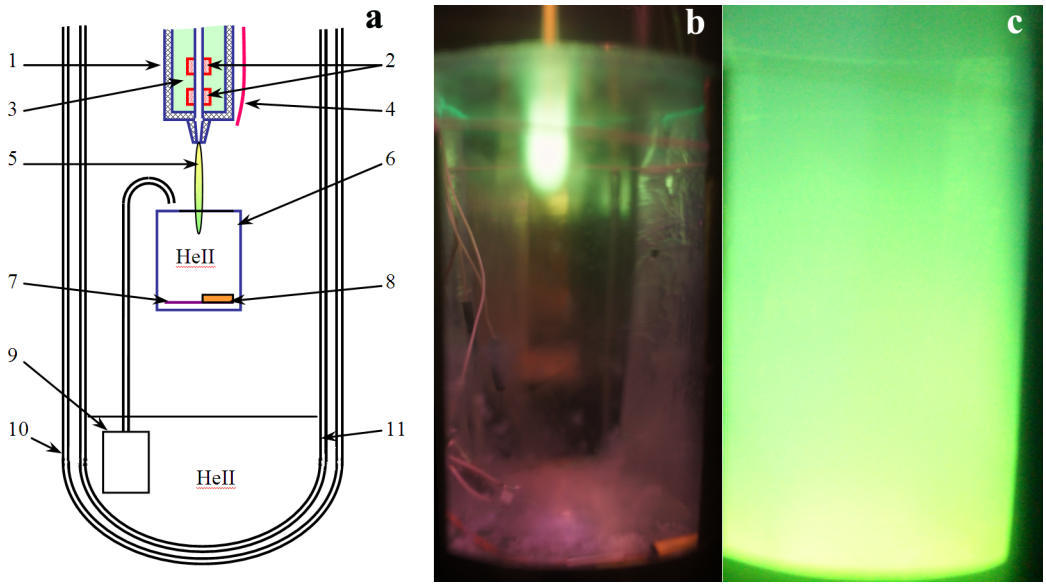

Figure 1. (a) Scheme of the cryogenic part of the experimental setup: 1, atom source; 2, electrodes for a RF discharge; 3, liquid nitrogen; 4, optical fiber; 5, gas jet; 6, beaker for sample condensation; 7, flat heater; 8, thermometer; 9, fountain pump in the main helium bath; 10, nitrogen dewar; 11, helium dewar. (b) Photo of the sample preparation process: a $[N_2]/[Xe]/[He] = 1/1/400$ gas mixture passed through a RF discharge is condensing in superfluid helium. (c) Photo of the flash during the sample destruction.

while the Vegard−Kaplan system of N_2 dominated in the spectra of condensates with a high content of xenon.

In this work, high local concentrations of nitrogen atoms (up to 10^{21} cm^{-3}) stabilized in xenon−nitrogen−helium condensates have been revealed by continuous wave electron spin resonance (CW ESR) spectroscopy of $N(^4S)$ atoms.

2. EXPERIMENTAL SETUP

The experimental technique of IHC sample preparation was first developed in 1974.[21] It is based on the injection of a helium gas jet containing impurity particles (Im = N, N_2, H, H_2, Ne, Ar, Kr, etc.) into bulk HeII. A gas mixture enters a helium bath region (Figure 1a) from a quartz capillary cooled with liquid nitrogen inside an atom source, as designated by position (pos.) 1 in Figure 1a. The lower portion of the capillary is surrounded by electrodes (pos. 2 in Figure 1a) to produce a RF discharge (f = 40−52 MHz, P = 40−90 W). The typical conditions during sample preparation were as follows: impurity admixture, $[Im]/[He] \sim 0.25-0.5\%$; gas jet flux, $(4.5-6) \times 10^{19}$ s^{-1}; superfluid helium temperature, 1.5 K; and duration of the sample condensation, 600−5000 s. The oxygen content in the gas mixtures is mainly a result of contamination of the helium gas. We employ helium gas with an oxygen content of ∼10 ppm. A gas jet (pos. 5 in Figure 1a) consisting of a mixture of helium and impurity gases was directed onto the surface of superfluid helium contained in a glass beaker (pos. 6 on Figure 1a) placed below the source at a distance of 20−35 mm. The steady-state level of HeII in the beaker (with an inner diameter of 40 mm) was maintained by a fountain pump situated in the main liquid helium bath. Superfluidity of bulk helium is essential for this method. Superfluid helium has a very high thermal conductivity, which is very important for preventing elevation of the temperature in the region of the entering jet containing atoms and nanoclusters. Superfluidity allows the formation of samples with high energy content by preventing thermal explosions if an occasional recombination of free radicals occurs during the process of sample formation.

Calibrated Lake Shore thermometers were used for the temperature measurements. A jet creates a crater on the HeII surface in the beaker (Figure 1b). The coldest part of the jet (inside the crater) is very distinct because of a bright white emission. The photo presented in Figure 1b was taken after a long preparation process (approximately 4200 s). The translucent condensate can be barely seen on the bottom of the beaker. Random flashes observed within the bulk HeII reveal the presence of a completely transparent condensate. The condensate became less transparent later during the process of sample compression because of the evaporation of liquid helium from the beaker.

Optical experiments have been carried out with two experimental setups possessing very similar cryogenic components, each including glass dewars for liquid nitrogen and helium, an atom source, a glass beaker for sample collection, and a fountain pump for maintaining the HeII supply in the beaker. The setup at Texas A&M University is described in more detail elsewhere.[22] The light emission from the sample passed through optical slits in both the helium and the nitrogen glass dewars and was collected by a lens into an optical fiber which splits into two separate channels, one of which was attached to an Ocean Optics spectrometer and the other to an Andor Shamrock SR500 spectrograph. The spectrometer allows spectrum capture rates up to 1000 full spectra/s (within the spectral range of 200−1100 nm). The optical resolution of the spectrometer was of order 1.3 nm (fwhm). The Andor spectrograph with an attached Newton EMCCD camera was used to obtain spectra with the higher spectral resolution (0.05 nm). The shortest exposition time is 3 ms. The glass dewars and beaker restricted the accessible spectral range to 310−1100 nm.

The setup in Chernogolovka was equipped with a vacuum feedthrough of an optical fiber for direct collection of light emitted by the impurity−helium sample (pos. 4 in Figure 1a). The open end of the fiber was directed into the beaker. The spectrometer AvaSpec-ULS2048XL-USB2 and the fibers were calibrated for absolute intensity measurements by a light source

dx.doi.org/10.1021/jp508534t | J. Phys. Chem. A 2015, 119, 2438−2448

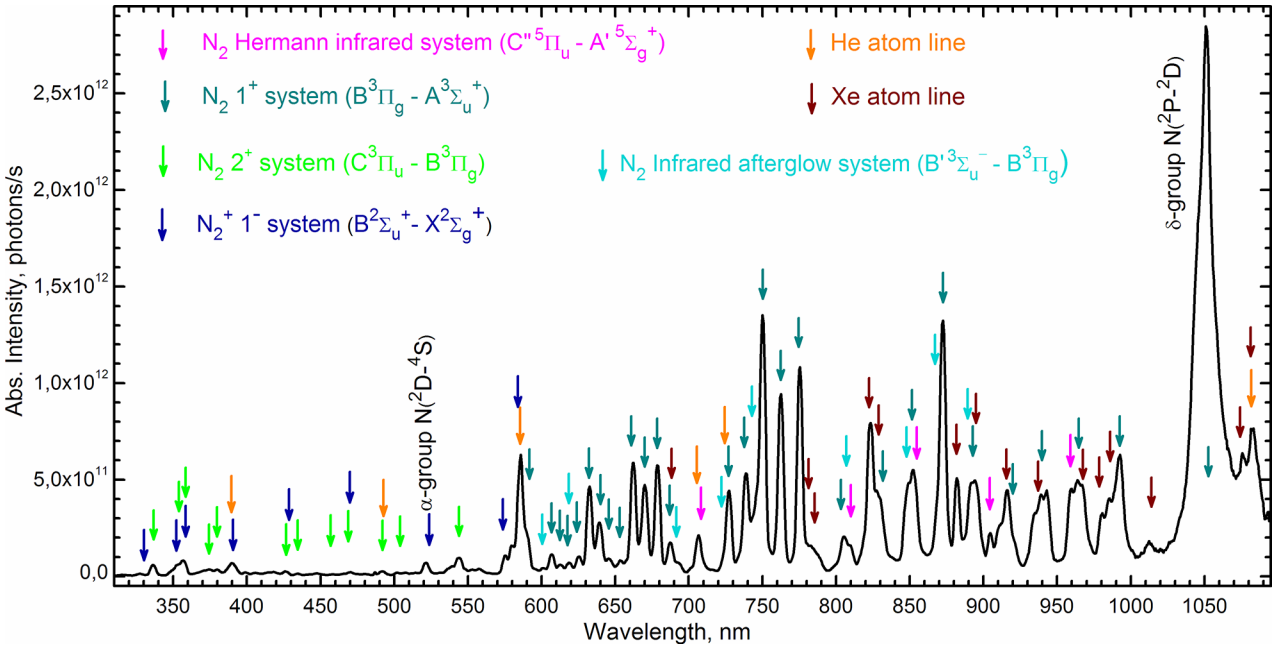

Figure 2. Luminescence spectrum (the absolute intensities of spectral lines and bands are given in photons per second) of the bottom part of the jet ([Xe]/[N_2]/[He] = 1/1/400 gas mixture passed through a RF discharge).

AvaLight-DH-BAL-CAL. The spectrometer allowed us to detect emissions within the spectral range from 200 to 1160 nm with resolution ~2.5 nm. The pressure of helium vapor in the dewar was measured with a RoseMount gauge S3051TA2 calibrated to work within the 0−10 kPa range.

The sample destruction process was started in HeII as the liquid helium level decreased in the beaker. When there was no liquid helium in the bottom part of the dewar, the presence of liquid helium in the beaker was revealed by the relation between the temperature measured in the beaker and the pressure detected in the helium dewar (the saturated helium vapor pressure). A bright flash shown in Figure 1c was observed at a temperature below 2 K (there was still some HeII below the flat heater). The pressure was about 400−500 Pa while liquid helium was still in the beaker and dropped down to a few pascals after the sample destruction. The temperature increased from 1.5 to 15−20 K during the sample destruction.

Electron spin resonance experiments were performed by using an experimental setup employing a metal cryostat designed for simultaneous magnetic resonance and optical investigations.[23] The sample preparation and ESR measurements were performed in a specially designed variable temperature insert which is situated in a Janis ^{4}He cryostat. The samples were prepared by using the discharge during a 10 min period of sample accumulation. The radio frequency discharge provided the atomic nitrogen through dissociation of N_2. These N atoms were captured in nanoclusters growing in the cold helium gas jet. The N−N_2−Xe−He nanoclusters were then collected at the bottom of the quartz beaker for ESR registration of stabilized N atoms. During ESR measurements, the temperature of the samples was stabilized at 1.35 K. The number of stabilized N(^{4}S) atoms was measured by comparing the double integrals of ESR atomic signals and a signal from a small ruby crystal that was used as a secondary standard. The ruby crystal was attached permanently to the bottom of the microwave cavity. The calibration of the absolute value of the number of spins in the ruby crystal was made by using a standard organic diphenyl-picrylhydrazyl (DPPH) sample with a known number ~2.4 × 10^{17} of spins. The atomic concentrations were calculated by dividing the number of atoms by the volume of the sample.

3. EXPERIMENTAL RESULTS

To study the localization of xenon−oxygen compounds and the processes of their excitation in the samples, we have studied the luminescence of xenon−oxygen complexes during destruction of samples containing different quantities of Xe, O, and N atoms trapped within nitrogen, xenon, and neon matrices. We also performed ESR studies of atoms stabilized in xenon−nitrogen−helium condensates for determining the main sources of energy stored in these condensates. The IHC samples were prepared by condensation of gas mixtures with different contents of xenon atoms: [Xe]/[N_2]/[He] = 10/1/2000, [Xe]/[N_2]/[He] = 5/1/1000, [Xe]/[N_2]/[He] = 1/1/400, [Xe]/[N_2]/[He] = 1/10/2000, and [Xe]/[N_2]/[Ne]/[He] = 1/1/10/4000. The oxygen content in a gas mixture was determined by the contamination of helium gas used in the experiments (≤10 ppm of O_2). To obtain some additional information concerning the structure of impurity clusters we also studied [N_2]/[He] = 1/100 and [Xe]/[N_2]/[He] = 50/1/10000 gas mixtures.

3.1. Luminescence Spectra during Sample Preparation. The luminescence spectrum obtained during sample preparation from the [Xe]/[N_2]/[He] = 1/1/400 gas mixture is shown in Figure 2. The most intense bands in this spectrum were assigned to the first positive, 1^+, system of N_2 (transitions $B^3\Pi_g$−$A^3\Sigma_u^+$) and the δ-group of atomic nitrogen (transition ^{2}P−^{2}D). The spectra of xenon−nitrogen−helium plasma jets are very rich because they contain bands of different systems of molecular nitrogen and lines of excited atoms of helium, xenon, and nitrogen. Beside the 1^+ system we have observed the second positive, 2^+ (transition $C^3\Pi_u$−$B^3\Pi_g$), Goldstein−Kaplan (transition $C'^3\Pi_u$−$B^3\Pi_g$), infrared afterglow (transition $B'^3\Sigma_u^-$−$B^3\Pi_g$), and Hermann infrared (transition $C''^5\Pi_u$−

dx.doi.org/10.1021/jp508534t | J. Phys. Chem. A 2015, 119, 2438−2448

$A^5\Sigma_g^+$) systems of molecular nitrogen, as well as the first negative, 1^-, system of the molecular ion N_2^+. There is also present the α-group of atomic nitrogen corresponding to the forbidden transition $^2D-^4S$ in the spectrum. The presence of the α- and δ-group reveals the clusters growing in the jet because the probabilities of the $^2D-^4S$ and $^2P-^2D$ transitions are greatly enhanced in a molecular nitrogen matrix.[24−26] The shape of the α-group spectrum and its position provide information on the clustering of the impurity particles in the jet. The α-group spectra detected with the higher spectral resolution from the bottom part of the jet for different gas mixtures are compared in Figure 3. As one can see, the shapes

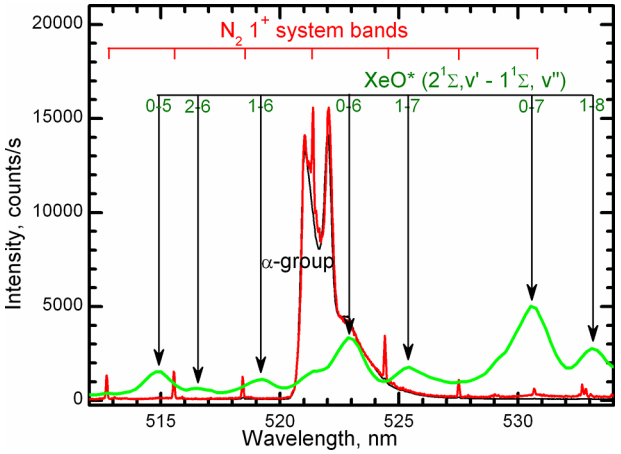

Figure 3. Comparison of the α-group spectra for different gas mixtures: black line, $[N_2]/[He]$ = 1/100; red line, $[Xe]/[N_2]/[He]$ = 1/1/400; and green line, $[Xe]/[N_2]/[He]$ = 50/1/10000.

of the α-group spectra are almost the same for the $[N_2]/[He]$ = 1/100 and $[Xe]/[N_2]/[He]$ = 1/1/400 gas mixtures, whereas no α-group was observed for a $[Xe]/[N_2]/[He]$ = 50/1/10000 gas mixture. The intensities of the spectra shown in Figure 3 were corrected for easier comparison of the α-group shapes. That is an additional reason why the band intensities of the N_2 1^+ system differ so much. Two other reasons are an enhancement of the emission of the 1^+ system N_2 in the nitrogen−xenon−helium gas mixture[27] and quenching of $N(^2D)$ atoms responsible for the α-group by xenon atoms.

3.2. Luminescence Spectra during Sample Destruction. The temporal dependencies of the integrated emission intensity, the temperature in the beaker, and the pressure in the cryostat during destruction of the sample condensed from the $[Xe]/[N_2]/[He]$ = 1/1/400 gas mixture are shown in Figure 4. The sample destruction process was initiated in HeII as the liquid helium level in the beaker decreased. Even though there was no liquid helium in the main helium bath, liquid helium remained only in the beaker because the temperature behavior in the beaker corresponded to the saturated helium vapor pressure. A vertical orange line corresponds to the time when all liquid helium has evaporated from the beaker (after this moment the pressure in the cryostat does not follow the saturated helium vapor pressure corresponding to the temperature in the beaker). A bright flash shown in Figure 1c was observed at a temperature below 2 K, at t = 323 s in Figure 4 (there was still some HeII below the flat heater). The spectrum of luminescence accompanying the sample destruction is shown in Figure 5 (red line). The luminescence spectra detected during the destructions of sample with higher xenon content

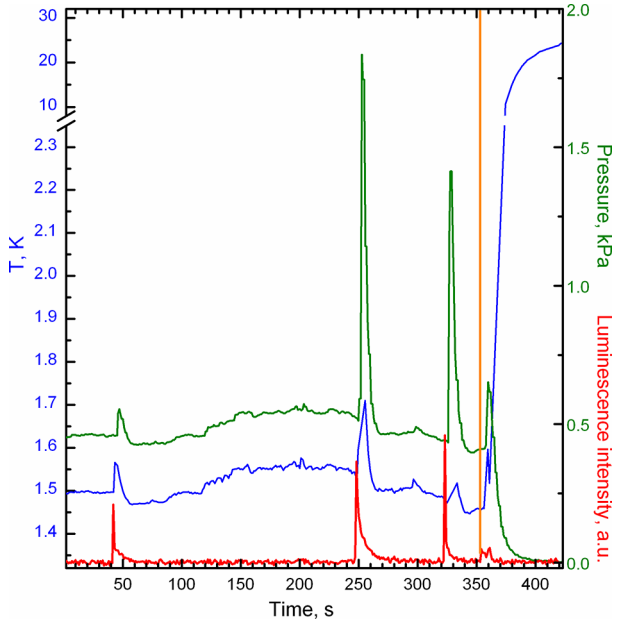

Figure 4. Temporal dependencies of the integrated luminescence intensity, the temperature in the beaker, and the pressure in the cryostat (red, blue, and green lines, respectively) during destruction of the sample condensed from the $[Xe]/[N_2]/[He]$ = 1/1/400 gas mixture. The orange line shows the time when liquid helium has completely evaporated from the beaker.

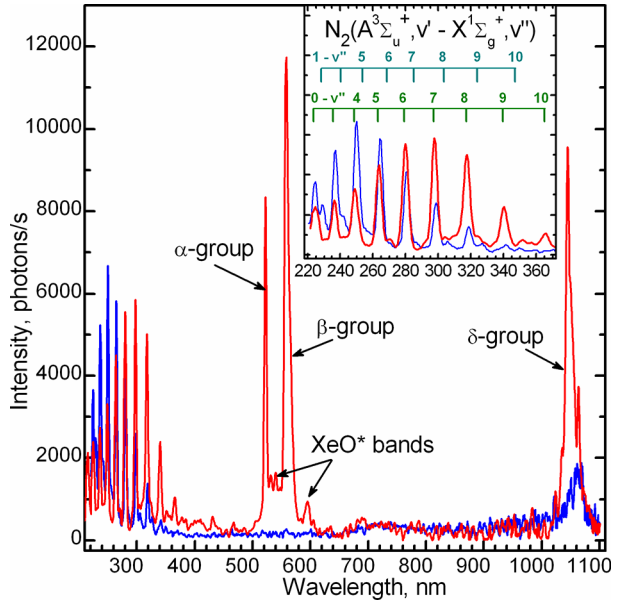

Figure 5. Luminescence spectra detected during the destruction of samples condensed from the $[Xe]/[N_2]/[He]$ = 1/1/400 (red line) and the $[Xe]/[N_2]/[He]$ = 5/1/1000 (blue line) gas mixtures. The UV parts of the spectra are shown in the inset.

(condensed from the $[Xe]/[N_2]/[He]$ = 5/1/1000 gas mixture, blue line) are also shown in Figure 5. The UV parts of the spectra are shown in detail in the inset. Both of the spectra were observed directly through optical fibers and corrected for the spectral response of the detection system. Both spectra presented in Figure 5 reveal the Vegard−Kaplan bands related to transitions $A^3\Sigma_u^+-X^1\Sigma_g^+$ of N_2. Decrease of the xenon content is manifested by the increasing intensity of

dx.doi.org/10.1021/jp508534t | J. Phys. Chem. A 2015, 119, 2438−2448

the α- and δ-groups of N atoms and β-group corresponding to the $^1S-^1D$ transition of O atoms.

Referring to Figure 5, some weak bands of the excimer molecule XeO* have also appeared in the spectrum of the sample condensed from the [Xe]/[N_2]/[He] = 1/1/400 gas mixture. The "green bands" correspond to the $2^1\Sigma,0-1^1\Sigma,v''$ transitions of XeO*,[5] whereas the broad peak at 595 nm can be associated with the transitions $Xe^+O^-(3^1\Sigma^+)-XeO(2^1\Sigma)$ or $XeO(2^1\Sigma-1^1\Delta)$.[10] Subsequent decrease of the xenon content is accompanied by a gain of the XeO* molecule emission. The luminescence spectra detected during the destruction of samples condensed from the [Xe]/[N_2]/[He] = 1/10/2000 (blue line) and the [Xe]/[N_2]/[Ne]/[He] = 1/1/10/4000 (red line) gas mixtures are shown in Figure 6. The glass dewars

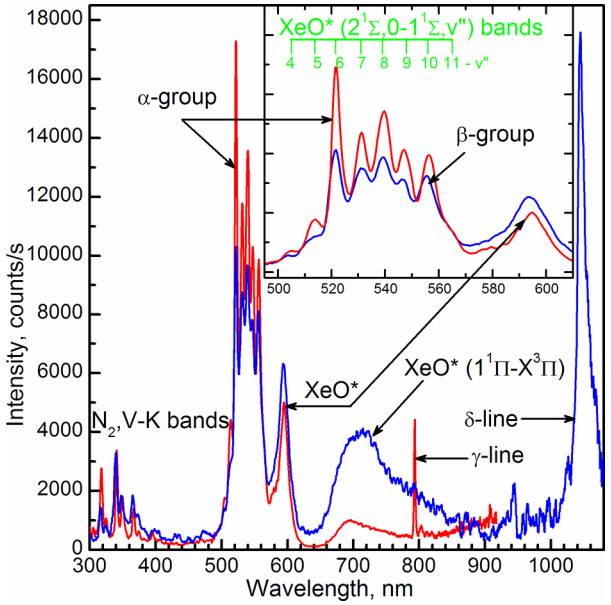

Figure 6. Luminescence spectra detected during the destruction of samples condensed from the [Xe]/[N_2]/[Ne]/[He] = 1/1/10/4000 (red line) and the [Xe]/[N_2]/[He] = 1/10/2000 (blue line) gas mixtures. The spectra of XeO* are shown in the inset.

cut off the emission for wavelengths shorter than 310 nm. The "green bands" of XeO* and their assignments are shown in the inset. The bands corresponding to the $2^1\Sigma,0-1^1\Sigma,6$ and $2^1\Sigma,0-1^1\Sigma,10$ transitions overlap with the α- and β-groups, respectively. The broad bands peaked at about 700 nm are also related to XeO* molecules.[10] The origin of these bands will be discussed in detail later.

It is worth noting the appearance at 793 nm of the so-called γ-line[28] which has been observed in solid N_2, argon, and neon,[28−31] but never in a xenon matrix. The origin of the γ-line is still unidentified.

We also studied the decay of the luminescence of a nitrogen−xenon−helium sample prepared from the [Xe]/[N_2]/[He] = 5/1/2000 gas mixture. For this sample we observed fast destruction during one intense flash. Figure 7 shows time dependence of the luminescence during destruction. The spectra were obtained by using the Andor spectrometer and Newton CCD camera with a time resolution of 3 ms. The luminescence covered the entire spectral range studied from 350 to 690 nm. In the spectrum of the largest flash, the Vegard−Kaplan bands of N_2 molecules, the "green bands" of XeO molecules, and α- and β-groups of N and O

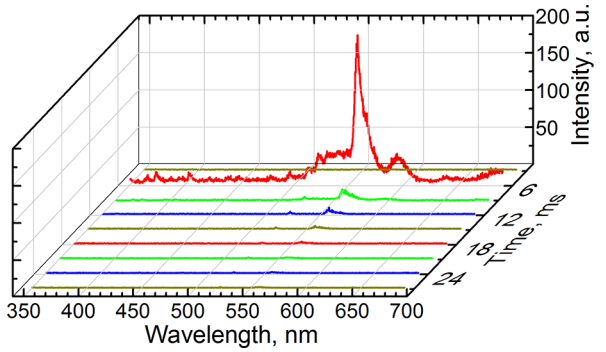

Figure 7. Dynamics of the luminescence spectra of nitrogen−xenon−helium sample during destruction. The sample was prepared from the [Xe]/[N_2]/[He] = 5/1/2000 gas mixture.

atoms are present. The figure shows that there is no luminescence from the sample before the main big flash. From the dynamics of the decay of the luminescence of the sample, we can see that in the spectrum which was taken 3 ms later than that of the main flash, only the weak Vegard−Kaplan bands of N_2 molecules as well as the α- and β-groups were present. Analysis of the decay of the emission of $N_2(A^3\Sigma_u^+)$ molecules gave the characteristic lifetime less than 3 ms.

3.3. ESR Investigations of Xenon−Nitrogen−Helium Samples. To understand the energy content in each of the samples, we performed ESR investigations. Figure 8 shows the

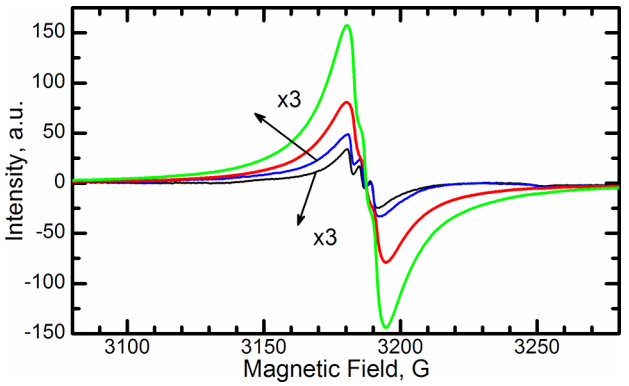

Figure 8. ESR spectra of N(^{4}S) atoms in nanoclusters prepared from different mixtures. Black, [Xe]/[N_2]/[He] = 50/1/10000; blue, [Xe]/[N_2]/[He] = 10/1/2000; red, [Xe]/[N_2]/[He] = 1/1/400; green, [Xe]/[N_2]/[He] = 1/10/2000. For better comparison, the intensities of the spectra for the former two mixtures were enlarged by a factor of 3.

ESR spectra of N atoms in as-prepared xenon−nitrogen−helium samples prepared from different gas mixtures. The calculated average concentrations of N atoms in the samples are listed in Table 1. From Table 1 we can see that with a greater relative content of N_2 in the gas mixture, the average concentration of N atoms stabilized in the samples increases, which indicates that N atoms are efficiently captured in the nitrogen−xenon nanoclusters. ESR spectra presented in Figure 8 have different shapes. We can see more resolved triplets in the spectra for the samples prepared from the gas mixtures with low content of N_2, while an increase of the broad features in the central region whose wings span about 100 G characterizes the samples prepared from the gas mixture with high N_2 content. The line width broadening definitely means that the local

dx.doi.org/10.1021/jp508534t | J. Phys. Chem. A 2015, 119, 2438−2448

Table 1. Average Concentration of N Atoms in Different Nitrogen−Xenon−Helium Samples

[Xe]/[N_2]/[He]	50/1/10000	10/1/2000	1/1/400	1/10/2000
average concentration (cm^{-3})	5.21×10^{17}	8.92×10^{17}	1.91×10^{18}	3.49×10^{18}

concentration of N atoms is very high and that the dipole−dipole interaction between neighboring spins dominates the spectra of the samples prepared from gas mixture with a high content of N_2. However, even for the sample with the highest content of N_2, i.e., [Xe]/[N_2]/[He] = 1/10/2000, there is still a barely observable triplet in the broad central region.

For a better understanding of the environment of trapped N atoms in the sample, we analyzed the ESR spectra using a combination of several simple functions. The values of the local concentrations of nitrogen atoms were obtained from the equation describing the line broadening due to dipole−dipole interaction valid for 3-D distributions. We tried to simulate shapes of the observed triplet for the atoms distributed over 3-D and 2-D spaces, and the best fit was always for a 3-D distribution. As an example, an analysis is presented in Figure 9

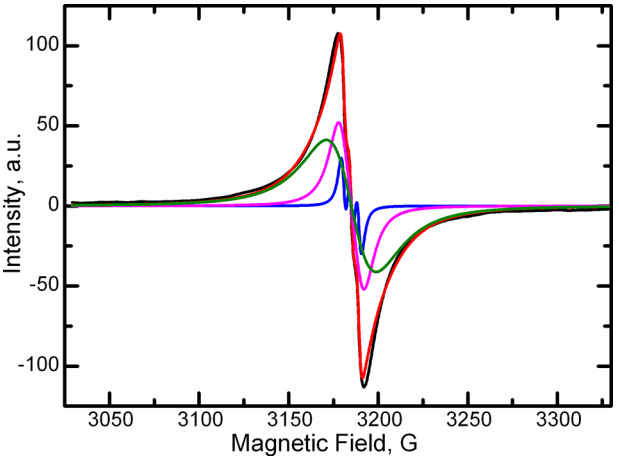

Figure 9. Experimental ESR spectrum of N atoms for an as-prepared xenon−nitrogen−helium sample condensed from the [Xe]/[N_2]/[He] = 1/1/400 gas mixture shown as a black line. The sum of the fitting lines is shown as a red line. Three triplets of fitting lines used for decomposing the experimental ESR spectrum are blue, triplet of Lorentzian lines with width 5.6 G; magenta, triplet of Lorentzian lines with width 16 G; and green, triplet of Lorentzian lines with width 45 G. The hyperfine splitting for all triplets is 4.2 G.

for the ESR spectrum of N atoms stabilized in xenon−nitrogen−helium sample prepared from the [Xe]/[N_2]/[He] = 1/1/400 gas mixture. We obtained a good fit for the experimental spectrum when we used a sum of three triplets of Lorentzian functions corresponding to the hyperfine components with spacing 4.2 G between the centers of each of these functions, but with different line widths: 5.6, 16, and 45 G. The ratio of double integrations corresponding to these Lorentzian triplets is about 1/8/34, which indicates that most of the N atoms are stabilized in the regions with high local concentrations: ∼19% with n_{loc}= 3.63×10^{20} cm^{-3} and 79% with n_{loc}= 10^{21} cm^{-3}. In a previous study,[17] we found that the nanoclusters with N_2 and Kr impurities have shell structures. The inner cores are mainly composed of Kr atoms, and the outer layers mostly consisted of N_2 molecules. Xe is also an inert atom which has an atomic number even larger than that of Kr. Therefore, the nanoclusters in the sample prepared from the mixture [Xe]/[N_2]/[He] should also exhibit a shell structure. As a result, the components with larger line width could be assigned to the N atoms located on the surface of the outer N_2 layer in the nanoclusters. As concerns the components with smaller line width, we cannot definitely assign them to N atoms in N_2 layers or those embedded inside the Xe cores. The ratio between the components indicates that more N atoms are residing in the regions with high local concentrations. A similar analysis was performed for all other ESR spectra obtained from different nitrogen−xenon−helium samples. The results of this analysis applied to the different samples are presented in Table 2.

4. DISCUSSION

Luminescence spectra of the nitrogen−helium plasma were thoroughly studied under different experimental conditions.[32−36] The luminescence of molecular nitrogen is enhanced because of the efficient energy transfer from metastable helium atoms and molecules resulting from the Penning ionization processes.[32,37] The addition of Xe atoms to the nitrogen−helium plasma further enhances and enriches the luminescence spectra of molecular nitrogen due to very efficient processes involving the pumping of nitrogen molecules from the ground $X^1\Sigma_g^+$ to the metastable state $A^3\Sigma_u^+$ by excited xenon atoms[27] and the energy pooling reaction of metastable $N_2(A^3\Sigma_u^+)$ molecules.[38,39] The energy pooling reactions efficiently produce N_2 molecules in the $C^3\Pi_u$ and $B^3\Pi_g$ states

Table 2. Results of Analysis of ESR Spectra of N Atoms for Different Samples

sample	components	linewidth (G)	hyperfine splitting (G)	local concentration (cm^{-3})	weight (%)
[Xe]/[N_2]/[He] = 50/1/10000	1	5.7	4.2	1.27×10^{20}	39
	2	18	4.2	4.09×10^{20}	61
[Xe]/[N_2]/[He] = 10/1/2000	1	5.7	4.2	1.27×10^{20}	13
	2	18	4.2	4.09×10^{20}	13
	3	30	4.2	6.81×10^{20}	74
[Xe]/[N_2]/[He] = 1/1/400	1	5.6	4.2	1.27×10^{20}	2.3
	2	16	4.2	3.63×10^{20}	18.6
	3	45	4.2	1.02×10^{21}	79.1
[Xe]/ [N_2]/ [He] = 1/10/2000	1	5.7	4.2	1.3×10^{20}	4
	2	16	4.2	3.63×10^{20}	23.5
	3	35	4.2	7.95×10^{20}	72.5

dx.doi.org/10.1021/jp508534t | J. Phys. Chem. A 2015, 119, 2438−2448

as products of reaction of two metastable $N_2(A^3\Sigma_u^+)$ molecules enhancing the emission of the 1^+ and 2^+ systems of molecular nitrogen (top reaction, ref 38; bottom reaction, ref 39):

$$N_2(A^3\Sigma_u^+) + N_2(A^3\Sigma_u^+) = N_2(C^3\Pi_u) + N_2(X^1\Sigma_g^+)$$

$$N_2(A^3\Sigma_u^+) + N_2(A^3\Sigma_u^+) = N_2(B^3\Pi_g) + N_2(X^1\Sigma_g^+)$$

For our experimental conditions just above the surface of superfluid helium, one can simultaneously observe a number of luminescent systems of molecular nitrogen. Such rich spectra, including bands of many (up to six) systems of N_2 and N_2^+, and atomic lines of helium and xenon, allow us to obtain detailed information for the kinetic modeling of processes occurring in the plasma,[40] and for theoretical simulations of emission spectra.[35,41] Moreover, the band identification became easier because the rotational structure is simpler at low jet temperatures (~10 K).

Appearance of the α-group in the jet spectrum reveals clustering processes.[26] Impurity particles (in the case of nitrogen atoms and molecules and xenon atoms) form nanoclusters upon rapid (within ~100 μs) cooling of the gaseous helium jet from 150 K down to 1.5 K.[42] The environment of $N(^2D)$ atoms captured in the nanoclusters affects the shape and intensity of the α-group spectrum.[43,44] Therefore, the similarity of the shapes of the α-group spectra detected from the samples condensed from $[N_2]/[He] = 1/100$ and $[Xe]/[N_2]/[He] = 1/1/400$ gas mixtures (Figure 3) seems rather unusual. The first of the possible explanations for this observation is the simplest because the α-group spectrum shapes might be expected to be the same for $N(^2D)$ atoms emitting from both N_2 and Xe environments. This suggestion is ruled out by the spectrum detected from a jet for the $[Xe]/[N_2]/[He] = 50/1/10000$ gas mixture. There is *no* α-group emission in this spectrum. The second explanation is in accordance with this fact: $N(^2D)$ atoms residing in a Xe matrix are deactivated without emitting radiation. There was no α-group observed from a xenon matrix doped with either nitrogen under excitation by protons and α-particles,[45] or NO under photoexcitation.[46] This experimental fact also confirms the second explanation. Such an effect of the xenon environment on metastable $N(^2D)$ atom contrasts sharply with the effect produced on the α-group spectrum shape and position by neon, argon, and krypton neighborhoods.[43,44] The addition of Ne, Ar, or Kr atoms to a nitrogen–helium gas mixture drastically changed the α-group spectrum shape and position. It is worth noting that there is no direct relation between the xenon content in a gas mixture and the δ-group intensity. The δ-group was rather intense in the luminescence spectra detected during destruction of each impurity–helium sample under study (it was detected also in the "red" spectra shown in Figure 6, but its intensity appears to be very weak because of the low sensitivity of the spectrometer in the range above 1 μm). We point out the fact of the absence of the α-group emission from xenon matrices[45,46] and IHCs with xenon as a main impurity (the spectra during condensation of the $[Xe]/[N_2]/[He] = 50/1/10000$ gas mixture, Figure 3, and destruction of the sample condensed from the $[Xe]/[N_2]/[He] = 5/1/1000$ gas mixture, Figure 5). A very weak α-group was observed from the bottom part of a gas jet during condensation of the $[Xe]/[N_2]/[He] = 1/1/400$ (Figure 2) gas mixture. It is about 50-fold less intense than the δ-group, corresponding the transition $N(^2P\text{-}^2D)$. The position of the α-group corresponds to $N(^2D)$ atoms in a matrix of molecular nitrogen. Much more intense α-groups are observed usually during condensation of nitrogen–helium jets passed through a RF discharge.[43] Addition of atoms of Ne, Ar, and Kr to nitrogen–helium gas mixtures is accompanied by further increase of the α-group intensity.[47] Interaction of xenon and metastable nitrogen atoms in the gas phase was studied before,[48−51] but no optical spectra of $N(^2D)$ and $N(^2P)$ atoms in a xenon matrix have yet been published.

Random flashes observed even within the HeII bulk during the sample accumulation in the beaker (Figure 1b) reveal the presence of a completely transparent condensate. The destruction of the samples began in the HeII bulk upon decreasing the HeII level in the beaker (the flashes in Figure 4). Luminescence spectra accompanying the sample destruction are related to the composition of each gas mixture used for sample preparation. The luminescence spectrum detected from the sample with the highest xenon content, prepared from a $[Xe]/[N_2]/[He] = 5/1/1000$ gas mixture, consists of the Vegard–Kaplan bands of N_2 molecules and the weak δ-group of N atoms (see Figure 5). The luminescence spectrum of the sample prepared from a $[Xe]/[N_2]/[He] = 1/1/400$ gas mixture consists mainly of the features specific for a nitrogen matrix: the intense α-, β-, and δ-groups and the Vegard–Kaplan bands. Only the Vegard–Kaplan bands of these features can be observed from a xenon matrix.[45] Nevertheless, the environment of $N_2(A^3\Sigma_u)$ molecules should be determined more accurately because the positions of the Vegard–Kaplan bands of N_2 in xenon and in molecular nitrogen matrices are almost identical (within of 0.2–0.4 nm) *in the case of good crystals*.[52] On the other hand, impurity clusters contain many structural defects,[53] which can affect the band positions. A key observation is the drastic difference of the $N_2(A^3\Sigma_u)$ lifetimes in these matrices. The lifetime of the $v = 0$ vibrational level of the $N_2(A^3\Sigma_u)$ molecules in a xenon matrix is about of 1 ms[45] in contrast to the much longer lifetime in a N_2 matrix, ~10 ms.[54] The fast decay of the Vegard–Kaplan bands (faster than 3 ms) observed in this work (see Figure 7) indicates that we observed $N_2(A^3\Sigma_u)$ molecules in a xenon matrix.

The very weak "green bands" of XeO* molecules corresponding to the $XeO(2^1\Sigma,0\text{–}1^1\Sigma,v'')$ transitions were also observed along with the accompanying broad band at 595 nm (Figure 5, red spectrum). The latter band is related either to the transition $Xe^+O^-(3^1\Sigma^+)\text{–}XeO(2^1\Sigma)$ or $XeO(2^1\Sigma\text{–}1^1\Delta)$.[10] The clustering of different impurities in the cold gas jet does not produce multishell clusters with perfectly sharp boundaries between a core and the shells; some particles with the lower polarizabilty can be trapped inside more polarizable impurities and vice versa.[15,17] This means that not only do oxygen and nitrogen atoms reside in a N_2 shell but also a small number can be captured inside the Xe core. Similarly, some Xe atoms can be located in a N_2 shell. Neighboring single xenon and oxygen atoms residing within a N_2 shell can also form excimer complexes due to energy transfer and UV photon absorption from excited particles during the process of sample destruction. The best candidate to be an emitter of UV photons and an energy bearer in a N_2 matrix is the molecule $N_2(A^3\Sigma_u)$ with the energy of the lowest excited level of about 6.2 eV.[52] As one can see in Figure 5, the strong bands of the Vegard–Kaplan system are observed in the UV range of the IHCs spectra. It is well-known that the metastable molecules $N_2(A^3\Sigma_u)$ transfer energy excitations very efficiently through the N_2 matrix.[55] To find a mechanism responsible for the energy transfer from $N_2(A^3\Sigma_u)$ molecules to xenon–oxygen complexes, we prepared

dx.doi.org/10.1021/jp508534t | J. Phys. Chem. A 2015, 119, 2438–2448

samples from [Xe]/[N_2]/[He] = 1/10/2000 and [Xe]/[N_2]/[Ne]/[He] = 1/1/10/4000 gas mixtures. We might expect efficient energy transfer within a N_2 matrix for the first sample and photoexcitation of XeO in the neon matrix in the second sample. Nevertheless, the positions of the Vegard−Kaplan bands observed were almost the same in both samples. The band positions of N_2 molecules emitting in a neon matrix should be blue-shifted by 2−3 nm[52] from the bands observed. While no emission from $A^3\Sigma_u$, $v' > 0$ should be observed in a neon matrix,[52,56] some weak bands from the $A^3\Sigma_u$, $v' = 1$ state were observable (Figure 6). These facts along with the similarity of the spectra of "green bands" for both samples support our suggestion that the emitting XeO* molecules reside in N_2 matrices. The resemblance of the XeO* spectra also observed during destruction of the sample prepared from a [Xe]/[N_2]/[Ne]/[He] = 1/1/10/4000 gas mixture does reveal a nitrogen matrix as the host of emitting molecules. The XeO* luminescence spectra from a neon matrix[10] are very similar to the ones observed in the gas phase[2] and differ from the spectra of XeO* molecules shown in Figures 5 and 6. The $1^1\Sigma$ state of an XeO* molecule hosted in a nitrogen matrix has larger vibrational quanta: seven bands (from 0−4 to 0−10 transitions) observed in our spectra cover the same spectral range (about 55 nm) as eight bands (from 0−4 to 0−11 transitions) in the spectra detected from XeO* in the gas phase, as well as in argon and neon matrices.[2,5,10] The absence of XeO* emission from a neon matrix in our experiment (see Figure 6) reflects the fact that photoexcitation of XeO complexes can be neglected as a possible source of excited XeO* molecules.

If a majority of an impurity cluster is composed of a thick nitrogen (or neon) shell or film, the density of xenon atoms within the shell or film is lower and more single xenon atoms reside next to oxygen atoms (because the ratio [O]/[Xe] for atoms trapped in clusters is given by the ratio [He]/[Xe] × 10^{-5} because of the oxygen contamination of helium gas used). The xenon−oxygen spectral features have been greatly enhanced in the luminescence spectra of the sample with lower relative xenon contents (compare Figures 5 and 6), which is in accordance with the above suggestion. The very broad band which peaked at 720 nm is a combination of two bands.[10] The first, at 690 nm, was associated with the transition ($1^1\Pi$−$X^3\Pi$) of the XeO* molecule.[10] The second band matches well to the spectrum produced by an O(^{1}S) atom at the xenon crystal surface.[8,12,57] This band was depleted (Figure 6) in the impurity clusters containing a xenon core and a neon shell with the nitrogen molecules and atoms distributed within the whole cluster. The sample consisting of such clusters had been prepared from a [Xe]/[N_2]/[Ne]/[He] = 1/1/10/4000 gas mixture.

We mention here that transitions from XeO*($2^1\Sigma$) in a xenon matrix have never been observed.[8,10] The energy of the ionic $Xe^+O^-(3^1\Sigma^+)$ state[58] is very close to 6.2 eV, which is the energy of the metastable molecule $N_2(A^3\Sigma_u)$. Such molecules are produced during destruction of impurity−helium condensates containing high densities of stabilized nitrogen atoms: N(^{4}S) + N(^{4}S) → N_2(A $^3\Sigma_u$). From the intense Vegard−Kaplan bands in the detected spectra, we have experimental confirmation of the high densities of $N_2(A^3\Sigma_u)$ molecules during the sample destruction. The $N_2(A^3\Sigma_u)$ molecules are also responsible for the excitation of N and O atoms:[55,59]

$$N_2(A^3\Sigma_u^+) + N(^4S) \rightarrow N(^2P) + N_2(X^1\Sigma_g^+) \quad (1)$$

$$N_2(A^3\Sigma_u^+) + N(^4S) \rightarrow N(^2P) + N_2(X^1\Sigma_g^+) \quad (2)$$

$$N_2(A^3\Sigma_u^+) + O(^3P) \rightarrow O(^1S) + N_2(X^1\Sigma_g^+) \quad (3)$$

The luminescence spectra contain the "fingerprints" of excited nitrogen and oxygen atoms as the α-, β-, and δ-groups. Therefore, we suggest that $N_2(A^3\Sigma_u)$ molecules are responsible for energy transfer to xenon−oxygen complexes which emit from the N_2 shells or films in impurity nanoclusters during destruction of impurity−helium condensates. Furthermore, we have assigned the spectra of the transitions XeO($2^1\Sigma$,0−$1^1\Sigma$,v″), observed in the present work and in our earlier study,[13] to xenon−oxygen complexes formed in N_2 matrices.

The optical spectra shown in the present work reveal many spectral features of xenon−oxygen molecules located in Xe and N_2 hosts (Figures 5 and 6), but none for nitrogen−xenon species. The existence of stable Xe−N bonds in neutral and ionic chemical compounds has been known for about 40 years. The first prepared compounds were rather complex and big molecules like $FXeN(SO_2F)_2$,[60] $Xe[N(SO_2F)_2]_2$,[61] $XeN(SO_2F)_2^+$, and $F[XeN(SO_2F)_2]_2^+$ cations.[62] Simpler molecules were theoretically predicted, and some of them were experimentally observed by the Helsinki group: HXeNC,[63] HXeNCO,[64] HCCXeNC,[65] ClXeNC, and BrXeNC.[66] It was shown that nitrogen atoms carry the main part of the negative charge in ClXeNC and BrXeNC molecules to form a stable bond with a "positive" xenon atom (partial atomic charges, −0.82, −0.81, and 0.94, 0.85, respectively).[66] Some years ago two new compounds containing a Xe−N bond, $XeNO_2^-$ and $XeNO_3^-$ anions, were theoretically predicted.[67] Possibly, the interaction between xenon and excited nitrogen atoms is not strong enough to form a simple XeN* molecule[48,49] with many bound states leading to rich spectra as an excimer molecule XeO* does. But this interaction leads to quenching of the ^{2}D and ^{2}P states of N atoms in a xenon matrix; we were able to observe only the weak red-shifted δ-group in the emission spectrum (Figure 5) of the sample prepared from [Xe]/[N_2]/[He] = 5/1/1000 gas mixtures. This quenching is more efficient than for the cases of the ^{1}S and ^{1}D states of O atoms, which in a xenon matrix produce bands at 370 and 740 nm.[8,12] We plan to study further the Xe−N interactions in impurity clusters stabilized in the HeII bulk.

ESR studies of nitrogen−xenon−helium samples provide additional evidence for the presence of high average and local concentrations of N atoms in the samples. All samples studied have regions with high local concentrations of N atoms. These regions are the source of the energy which was released during chain reactions of stabilized N atoms. Part of this energy was transferred to excite atoms and molecules observed in luminescence spectra during sample destruction.

More detailed analysis of the ESR spectra provides information about the environment of the stabilized N atoms and their local concentrations in the nanoclusters. It was found that there are three different regions (layers) in nitrogen−xenon nanoclusters with relatively low (1.27×10^{20} cm^{-3}), medium ($(3.6-4) \times 10^{20}$ cm^{-3}), and high ($(7-10) \times 10^{20}$ cm^{-3}) local concentrations of N atoms. The best fits to the experimental ESR lines were observed for the hyperfine splitting 4.2 G, which is equal to that for N atoms in substitutional sites in N_2 matrices.[68,69] The values of hyperfine splitting for N atoms in Xe matrices are in the range of 4.3−4.4 G.[46,69,70] It should be mentioned that only the analysis of the resolved triplet in the ESR spectra is sensitive to the value of

dx.doi.org/10.1021/jp508534t | J. Phys. Chem. A 2015, 119, 2438−2448

the hyperfine splitting. The broad features of the spectra are less sensitive to the value of the hyperfine splitting. In our previous studies of N atoms in nitrogen−krypton−helium samples, it was found that broad features of the ESR spectra of N atoms correspond to atoms stabilized in N_2 molecular layers where most of the atoms resided.[17] Only a small portion of the atoms were stabilized in the krypton core of the nanoclusters. From the ESR spectra of N atoms in xenon−nitrogen−helium samples we did not find N atoms in a Xe matrix. This means that the number of N atoms in the Xe environment is at least 1 order of magnitude less than that in the N_2 environment.

5. CONCLUSIONS

(1.) The xenon−nitrogen−helium condensates immersed in superfluid helium were studied by optical and ESR spectroscopies. Average and local concentrations of stabilized nitrogen atoms in xenon−nitrogen−helium samples were determined. Very high local densities of nitrogen atoms (up to 10^{21} cm^{-3}) were obtained in xenon−nitrogen nanoclusters.

(2.) Luminescence from the collection xenon−nitrogen nanoclusters containing stabilized N and O atoms were studied during explosive destruction of the samples. An emission of excimer XeO* molecules in molecular nitrogen films has been observed for the first time.

(3.) A Vegard−Kaplan emission of N_2 molecules was observed from Xe cores of nanoclusters. This was determined from the decay measurements (τ < 3 ms).

(4.) The mechanism of excitation of xenon−oxygen complexes during destruction of xenon−nitrogen−helium samples was revealed. Recombination of nitrogen atoms stabilized within impurity nanoclusters produce metastable $N_2(A^3\Sigma_u)$ molecules which are responsible for energy transfer to the xenon−oxygen complexes emitting during destruction of impurity−helium condensates.

AUTHOR INFORMATION

Corresponding Author

*E-mail: khmel@physics.tamu.edu. Tel.: (979)4587943.

Notes

The authors declare no competing financial interest.

ACKNOWLEDGMENTS

This study was supported by the Program "Matter at high energy densities" of the Presidium of the Russian Academy of Sciences and by NSF Grant DMR 1209255.

REFERENCES

(1) Kenty, C.; Aicher, J. O.; Noel, E. B.; Poritsky, A.; Paolino, V. A New Band System in the Green Excited in a Mixture of Xenon and Oxygen and the Energy of Dissociation of CO. *Phys. Rev.* **1946**, *69*, 36−37.

(2) Cooper, C. D.; Cobb, G. C.; Tolnas, E. L. Visible Spectra of XeO and KrO*. *J. Mol. Spectrosc.* **1961**, *7*, 223−230.

(3) Cunningham, D. L.; Clark, K. C. Rates of Collision-Induced Emission from Metastable O(^{1}S) Atoms. *J. Chem. Phys.* **1974**, *61*, 1118−1124.

(4) Simmons, J. D.; Maki, A. D.; Hougen, J. T. Spectroscopic Analysis of the $d^1\Sigma^+ \rightarrow a^1\Sigma^+$ and $d^1\Sigma^+ \rightarrow b^1\Pi^+$ Green Band Systems of XeO. *J. Mol. Spectrosc.* **1979**, *74*, 70−101.

(5) Goodman, J.; Tully, J. C.; Bondybey, V. E.; Brus, L. E. Excited State Spectroscopy, Subpicosecond Predissociation, and Solvation of Diatomic XeO in Solid Rare Gas Hosts. *J. Chem. Phys.* **1977**, *66*, 4802−4810.

(6) Monahan, K. M.; Rehn, V. Energy Transfer in Solid Xe and Kr Doped with N_2O. *J. Chem. Phys.* **1978**, *68*, 3814−3817.

(7) Yurtaeva, E. M.; Fugol', I. Ya.; Belov, A. G. Spectroscopic Study of Rydberg States of Excimer Molecules of Noble Gases and Oxygen. *Sov. J. Low Temp. Phys.* **1990**, *16*, 54−64.

(8) Lawrence, W. G.; Apkarian, V. A. Electronic Spectroscopy of Oxygen Atoms Trapped in Solid Xenon. *J. Chem. Phys.* **1992**, *97*, 2229−2236.

(9) Lawrence, W. G.; Apkarian, V. A. Two-Photon Induced Exciton Mediated Dissociation of N_2O and Photomobility of O Atoms in Crystalline Xe. *J. Chem. Phys.* **1992**, *97*, 6199−6207.

(10) Belov, A. G.; Yurtaeva, E. M. Xenon Excimer Compounds with Oxygen in Inert-gas Crystal Matrices. *Low Temp. Phys.* **2001**, *27*, 938−948.

(11) Loree, T. R.; Showalter, R. R.; Johnson, T. M.; Birmingham, B. S.; Hughes, W. M. Lasing XeO in Liquid Argon. *Opt. Lett.* **1986**, *11*, 510−512.

(12) LeClair, L. R.; McConkey, J. W. Selective Detection of O(^{1}S) Following Electron Impact Dissociation of O_2 and N_2O using a XeO* Conversion Technique. *J. Chem. Phys.* **1993**, *99*, 4566−4577.

(13) Boltnev, R. E.; Krushinskaya, I. N.; Pelmenev, A. A.; Stolyarov, D. Yu.; Khmelenko, V. V. The Thermoluminescence Spectra Obtained on the Destruction of Impurity-Helium Solid Phase Samples. *Chem. Phys. Lett.* **1999**, *305*, 217−224.

(14) Kiselev, S. I.; Khmelenko, V. V.; Lee, D. M.; Kiryukhin, V.; Boltnev, R. E.; Gordon, E. B.; Keimer, B. Structural Studies of Impurity-Helium Solids. *Phys. Rev. B* **2001**, *65*, 024517−12.

(15) Boltnev, R. E.; Jarvinen, J.; Bernard, E. P.; Khmelenko, V. V.; Lee, D. M. Stabilization of Hydrogen Atoms in Aggregates of Krypton Nanoclusters Immersed in Superfluid Helium. *Phys. Rev. B* **2009**, *79*, 180506(R)−4.

(16) Boltnev, R. E.; Khmelenko, V. V.; Lee, D. M. Stabilization of H and D atoms in Krypton-Helium Nanocondensates. *Low Temp. Phys.* **2010**, *36*, 484−494.

(17) Mao, S.; Boltnev, R. E.; Khmelenko, V. V.; Lee, D. M. ESR Studies of Nitrogen Atoms Stabilized in Aggregates of Krypton-Nitrogen Nanoclusters Immersed in Superfluid Helium. *Low Temp. Phys.* **2012**, *38*, 1037−1043.

(18) Khmelenko, V. V.; Pelmenev, A. A.; Krushinskaya, I. N.; Bykhalo, I. B.; Boltnev, R. E.; Lee, D. M. Energy Release Channels during Destruction of Impurity-Helium Condensates. *J. Low Temp. Phys.* **2013**, *171*, 302−308.

(19) Danylchenko, O. G.; Doronin, Yu. S.; Kovalenko, S. I.; Samovarov, V. N. Phase Separation into Pure Components in Mixed Ar-Xe Clusters. *JETP Lett.* **2006**, *84*, 324−328.

(20) Laarmann, T.; Wabnitz, H.; von Haeften, K.; Möller, T. Photochemical Processes in Doped Argon-Neon Core-Shell Clusters: The Effect of Cage Size on the Dissociation of Molecular Oxygen. *J. Chem. Phys.* **2008**, *128*, 014502.

(21) Gordon, E. B.; Mezhov-Deglin, L. P.; Pugachev, O. F. Stabilization of Nitrogen Atoms in Superfluid Helium. *JETP Lett.* **1974**, *19*, 63−65.

(22) Khmelenko, V. V.; Mao, S.; Meraki, A.; Wilde, S. C.; McColgan, P.; Boltnev, R. E.; Pelmenev, A. A.; Lee, D. M. Luminescence of Oxygen Atoms Stimulated by Metastable Helium at Cryogenic Temperatures. *Phys. Rev. Lett.* **2013**, *111*, 183002.

(23) Mao, S.; Meraki, A.; McColgan, P. T.; Shemelin, V.; Khmelenko, V. V.; Lee, D. M. Experimental Setup for Investigation of Nanoclusters at Cryogenic Temperatures by Electron Spin Resonance and Optical Spectroscopies. *Rev. Sci. Instrum.* **2014**, *85*, 073906.

(24) Herzfeld, C. M.; Broida, H. P. Interpretation of Spectra of Atoms and Molecules in Solid Nitrogen Condensed at 4.2 K. *Phys. Rev.* **1956**, *101*, 606−612.

(25) Kunsch, P. L.; Dressler, K. Calculation of Dynamically Induced Electronic Transitions of Matrix-Isolated Atomic Nitrogen. *J. Chem. Phys.* **1978**, *68*, 2550−2561.

(26) Popov, E. A.; Eloranta, J.; Ahokas, J.; Kunttu, H. On the Formation Mechanism of Impurity−Helium Solids: Evidence for Extensive Clustering. *Low Temp. Phys.* **2003**, *29*, 510−514.

(27) Sadeghi, N.; Setser, D. W. Primary $N_2(B)$ Vibrational Distributions from Excitation-Transfer Reactions between $Kr(^3P_2)$ or $Xe(^3P_2)$ Atoms and N_2. *Chem. Phys. Lett.* **1981**, *82*, 44−50.
(28) Peyron, M.; Broida, H. P. Spectra Emitted from Solid Nitrogen Condensed at Very Low Temperatures from a Gas Discharge. *J. Chem. Phys.* **1959**, *30*, 139−150.
(29) Horl, E. M. Light Emission from Solid Nitrogen during and after Electron Bombardment. *J. Mol. Spectrosc.* **1959**, *3*, 425−449.
(30) Tian, R.; Michl, J. Fast-Particle Bombardment of Solid Nitrogen. *Faraday Discuss. Chem. Soc.* **1988**, *86*, 113−124.
(31) Shoen, L. J.; Broida, H. P. Spectra Emitted from Rare Gas-Oxygen Solids during Electron Bombardment. *J. Chem. Phys.* **1960**, *32*, 1184−1193.
(32) Richardson, W. C.; Setser, D. W. Penning Ionization Optical Spectroscopy: Metastable Helium (He 2^3S) Atoms with Nitrogen, Carbon Monoxide, Oxygen, Hydrogen Chloride, Hydrogen Bromide, and Chlorine. *J. Chem. Phys.* **1973**, *58*, 1809−1825.
(33) Myers, G.; Cunningham, A. J. Quenching Reactions of $He(2^3S)$ and $He_2(2^3\Sigma)$ Metastables in the Presence of N_2 and O_2. *J. Chem. Phys.* **1977**, *67*, 3352−3359.
(34) Pouvesle, J. M.; Stevefelt, J.; Collins, C. B. Study of Two-Body and Three-Body Channels for the Reaction of Metastable Helium Atoms with Nitrogen. *J. Chem. Phys.* **1985**, *82*, 2274−2279.
(35) Martus, K.; Masoud, N.; Becker, K. Collisional and Radiative Processes in High-Pressure Ne/N_2 Discharges. *Plasma Sources Sci. Technol.* **2006**, *15*, 84−90.
(36) Shakhatov, V. A.; Lebedev, Yu. A. Radiation Spectroscopy in the Study of the Influence of a Helium-Nitrogen Mixture Composition on Parameters of DC Glow Discharge and Microwave Discharge. *High Temp.* **2012**, *50*, 658−683.
(37) Druyvesteyn, M. J.; Penning, F. M. The Mechanism of Electrical Discharges in Gases of Low Pressure. *Rev. Mod. Phys.* **1940**, *12*, 87−174.
(38) Stedman, D. H.; Setser, D. W. Energy Pooling by Triplet Nitrogen $(A^3\Sigma_u^+)$ Molecules. *J. Chem. Phys.* **1969**, *50*, 2256−2258.
(39) Piper, L. G. State-to-State N_2 $(A^3\Sigma^+_u)$ Energy Pooling Reactions. II. The Formation and Quenching of N_2 $(B\ ^3\Pi_g, v' = 1-12)$. *J. Chem. Phys.* **1988**, *88*, 6911−6921.
(40) Guerra, V.; Sa, P. A.; Loureiro, J. Kinetic Modeling of Low-Pressure Nitrogen Discharges and Post-Discharges. *Eur. Phys. J.: Appl. Phys.* **2004**, *28*, 125−152.
(41) Cicala, G.; De Tommaso, E.; Raino, A. C.; Lebedev, Yu. A.; Shakhatov, V. A. Study of Positive Column of Glow Discharge in Nitrogen by Optical Emission Spectroscopy and Numerical Simulation. *Plasma Sources Sci. Technol.* **2009**, *18*, 025032.
(42) Kiryukhin, V.; Bernard, E. P.; Khmelenko, V. V.; Boltnev, R. E.; Krainyukova, N. V.; Lee, D. M. Noble Gas Nanoclusters with Five-fold Symmetry Stabilized in Superfluid Helium. *Phys. Rev. Lett.* **2007**, *98*, 195506.
(43) Boltnev, R. E.; Gordon, E. B.; Khmelenko, V. V.; Krushinskaya, I. N.; Martynenko, M. V.; Pelmenev, A. A.; Popov, E. A.; Shestakov, A. F. Luminescence of Nitrogen and Neon Atoms Isolated in Solid Helium. *Chem. Phys.* **1994**, *189*, 367−382.
(44) Boltnev, R. E.; Gordon, E. B.; Khmelenko, V. V.; Martynenko, M. V.; Popov, E. A.; Pelmenev, A. A.; Shestakov, A. F. The Metastable Ne $(^3P_2)$ and N (^2D) Atoms in Cores of Solitary and Sticking Helium Clusters: Helium Surrounding and Heavy Neighbor Influence. *J. Chim. Phys. Phys.-Chim. Biol.* **1995**, *92*, 362−383.
(45) Berg, L. E.; Lindblom, P.; Olsson, T.; Aho, K.; Hallsten, U.; Solin, O. Excitation of Oxygen and Nitrogen in Solid Krypton and Xenon Using Ion Beam Irradiation. *J. Phys. B: At., Mol. Opt. Phys.* **1994**, *27*, 5241−5250.
(46) Eloranta, J.; Vaskonen, K.; Hakkanen, H.; Kiljunen, T.; Kunttu, H. 193 nm Photodynamics of NO in Rare Gas Matrices: Fluorescence, Thermoluminescence and Photodissociation. *J. Chem. Phys.* **1998**, *109*, 7784−7792.
(47) Khmelenko, V. V.; Krushinskaya, I. N.; Boltnev, R. E.; Bykhalo, I. B.; Pelmenev, A. A.; Lee, D. M. Dynamics of Thermoluminescence Spectra of Impurity-Helium Condensates Containing Stabilized Nitrogen and Oxygen Atoms. *Low Temp. Phys.* **2012**, *38*, 688−699.
(48) Herman, L.; Herman, R. New Afterglow Emission Associated with Metastable Nitrogen Atoms. *Nature (London, U.K.)* **1961**, *191*, 346−347.
(49) Herman, L.; Herman, R. Rotational Structure of the 4925 Å. Band System of the XeN Molecule. *Nature (London, U.K.)* **1962**, *193*, 156−157.
(50) Vilesov, A. F.; Pravilov, A. M.; Smirnova, L. G. XeN Excimer. *Opt. Spektrosk.* **1988**, *65*, 896−898.
(51) Vilesov, A. F.; Wildt, J.; Fink, E. H. Emission of Xe-N(^{2}P) Collision Complexes near the N(^{2}P-^{2}D) Lines. *Chem. Phys.* **1991**, *153*, 531−537.
(52) Poltoratski, Yu. B.; Fugol, I. Ya. A Study of the Excited Triplet State of Nitrogen $(A^3\Sigma_u^+)$ in Cryocrystals. *Sov. J. Low Temp. Phys.* **1979**, *5*, 439−449.
(53) Kiryukhin, V.; Keimer, B.; Boltnev, R. E.; Khmelenko, V. V.; Gordon, E. B. Intert-Gas Solids with Nanoscale Porosity. *Phys. Rev. Lett.* **1997**, *79*, 1774−1777.
(54) Zumofen, G.; Loher, M.; Dressler, K. Dispersive Transport and Multiple Trapping in Solid N_2. *J. Lumin.* **1988**, *40&41*, 191−192.
(55) Oehler, O.; Smith, D. A.; Dressler, K. Luminescence Spectra of Solid Nitrogen Excited by Electron Impact. *J. Chem. Phys.* **1977**, *66*, 2097−2107.
(56) Tinti, D. S.; Robinson, G. W. Spectroscopic Evidence for Slow Vibrational and Electronic Relaxation in Solids. The Vegard−Kaplan and Second Positive Systems of N_2 in Solid Rare Gases. *J. Chem. Phys.* **1968**, *49*, 3229−3245.
(57) Kedzierski, W.; Blejdea, E.; DiCarlo, A.; McConkey, J. W. Metastable Oxygen Atom Detection Using Rare Gas Matrices. *J. Phys. B: At., Mol. Opt. Phys.* **2010**, *43*, 085204−4.
(58) Yamanishi, M.; Hirao, K.; Yamashita, K. Theoretical Study of the Low-Lying Electronic States of XeO and XeS. *J. Chem. Phys.* **1998**, *108*, 1514−1521.
(59) Piper, L. G. The Excitation of N(^{2}P) by $N_2(A\ ^3\Sigma_u^+, v' = 0,1)$. *J. Chem. Phys.* **1989**, *90*, 7087−7095.
(60) LeBlond, R. D.; DesMarteau, D. D. Fluoro[imidobis(sulphuryl fluoride)]xenon. An Example of a Xenon−Nitrogen Bond. *J. Chem. Soc., Chem. Commun.* **1974**, 555−556.
(61) DesMarteau, D. D.; LeBlond, R. D.; Hassain, S. F.; Nothe, D. Xenon−Nitrogen Bonds. The Synthesis and Characterization of [Imidobis(sulfuryl fluoride)]xenon(II) Derivatives $Xe[N(SO_2F)_2]_2$, $FXeN(SO_2F)_2$, and $[(FSO_2)_2NXe]_2F^+AsF_6^-$ and the Radical $\cdot N(SO_2F)_2$. *J. Am. Chem. Soc.* **1981**, *103*, 7734−7739.
(62) Faggiani, R.; Kennepohl, D. K.; Lock, C. J. L.; Schrobilgen, G. J. The $XeN(SO_2F)_2^+$ and $F[XeN(SO_2F)_2]_2^+$ Cations: Synthesis and X-ray Structure of $XeN(SO_2F)_2{}^+Sb_3F_{16}^-$ and Raman and Multinuclear Magnetic Resonance Studies of the AsF_6^- and $Sb_3F_{16}^-$ Compounds. *Inorg. Chem.* **1986**, *25*, 563−571.
(63) Pettersson, M.; Lundell, J.; Khriachtchev, L.; Räsänen, M. Neutral Rare-gas Containing Charge-transfer Molecules in Solid Matrices. III. HXeCN, HXeNC, and HKrCN in Kr and Xe. *J. Chem. Phys.* **1998**, *109*, 618−625.
(64) Pettersson, M.; Khriachtchev, L.; Lundell, J.; Jolkkonen, S.; Räsänen, M. Photochemistry of HNCO in Solid Xenon: Photoinduced and Thermally Activated Formation of HXeNCO. *J. Phys. Chem. A* **2000**, *104*, 3579−3583.
(65) Khriachtchev, L.; Lignell, A.; Tanskanen, H.; Lundell, J.; Kiljunen, H.; Räsänen, M. Insertion of Noble Gas Atoms into Cyanoacetylene: An ab Initio and Matrix Isolation Study. *J. Phys. Chem. A* **2006**, *110*, 11876−11885.
(66) Arppe, T.; Khriachtchev, L.; Lignell, A.; Domanskaya, A. V.; Räsänen, M. Halogenated Xenon Cyanides ClXeCN, ClXeNC, and BrXeCN. *Inorg. Chem.* **2012**, *51*, 4398−4402.
(67) Sun, Y.-L.; Hong, J.-T.; Hu, W.-P. Theoretical Prediction of Stable Noble-Gas Anions $XeNO_2^-$ and $XeNO_3^-$ with very Short Xenon-Nitrogen Bond Lengths. *J. Phys. Chem. A* **2010**, *114*, 9359−9367.

(68) Dmitriev, Yu.; Zhitnikov, R. A. EPR Studies of N, H, and D Atoms Trapped in the Matrix of Solid Molecular Nitrogen. *Low Temp. Phys.* **1998**, *24*, 44−49.
(69) Fisher, P. H. H.; Charles, S. W.; McDowell, C. A. Electron Spin Resonance Study of the Photolytic Decomposition of HN_3 in Inert Matrices at 4.2 K. *J. Chem. Phys.* **1967**, *46*, 2162−2166.
(70) Jackel, C. S.; Nelson, W. H.; Gordy, W. Matrix Perturbations of the ESR of Trapped H, N, P, and As Atoms at 4.2 K. *Phys. Rev.* **1968**, *176*, 453−460.